molecules

MDPI

Article

Al-Decorated C_2N Monolayer as a Potential Catalyst for NO Reduction with CO Molecules: A DFT Investigation

Xinmiao Liu †, Yunjie Xu † and Li Sheng *

MIIT Key Laboratory of Critical Materials Technology for New Energy Conversion and Storage, School of Chemistry and Chemical Engineering, Harbin Institute of Technology, Harbin 150001, China
* Correspondence: shengli@hit.edu.cn
† These authors contributed equally to this work.

Abstract: Developing efficient and economical catalysts for NO reduction is of great interest. Herein, the catalytic reduction of NO molecules on an Al-decorated C_2N monolayer (Al-C_2N) is systematically investigated using density functional theory (DFT) calculations. Our results reveal that the Al-C_2N catalyst is highly selective for NO, more so than CO, according to the values of the adsorption energy and charge transfer. The NO reduction reaction more preferably undergoes the $(NO)_2$ dimer reduction process instead of the NO direct decomposition process. For the $(NO)_2$ dimer reduction process, two NO molecules initially co-adsorb to form $(NO)_2$ dimers, followed by decomposition into N_2O and O_{ads} species. On this basis, five kinds of $(NO)_2$ dimer structures that initiate four reaction paths are explored on the Al-C_2N surface. Particularly, the cis-$(NO)_2$ dimer structures ($D_{cis\text{-}N}$ and $D_{cis\text{-}O}$) are crucial intermediates for NO reduction, where the max energy barrier along the energetically most favorable pathway (path II) is as low as 3.6 kcal/mol. The remaining O_{ads} species on Al-C_2N are then easily reduced with CO molecules, being beneficial for a new catalytic cycle. These results, combined with its low-cost nature, render Al-C_2N a promising catalyst for NO reduction under mild conditions.

Keywords: NO catalytic reduction; C_2N monolayer; Al-C_2N catalyst; nitric oxide; DFT calculation

Citation: Liu, X.; Xu, Y.; Sheng, L. Al-Decorated C_2N Monolayer as a Potential Catalyst for NO Reduction with CO Molecules: A DFT Investigation. *Molecules* **2022**, *27*, 5790. https://doi.org/10.3390/molecules27185790

Academic Editor: Mauricio Alcolea Palafox

Received: 27 July 2022
Accepted: 4 September 2022
Published: 7 September 2022

1. Introduction

The increasing emission of nitrogen oxides (NO_x) has brought serious harm to the atmospheric environment and human health [1–3]. Nitric oxide (NO), which comprises approximately 95% of NO_x emissions, is considered a major cause of acid rain and photochemical smog formation [4]. Selective catalytic reduction (SCR) is a promising method that typically selects CO [5–9], H_2 [8–11], or NH_3 [12] as the reducing agent to eliminate emitted NO. Since CO and NO commonly coexist in exhaust gases, the catalytic reduction of NO with CO as a reducing agent can simultaneously convert CO and NO pollutants into harmless N_2 and acceptable CO_2. Noble metal catalysts such as Pt, Au, or Pd have been extensively studied; however, there are problems, such as high cost, low abundance, and toxicity [13–16]. Thus, it is of utmost importance to design high-efficiency and low-cost alternative catalysts to remove or reduce NO molecules.

Reducing the particle size of active metals to a few atoms is a valuable strategy to improve catalytic activity [17–20]. Compared to traditional catalysts, single-atom catalysts can greatly decrease the amount of metal used, thereby reducing costs. In particular, single-atom catalysts have been proven to efficiently catalyze or adsorb various harmful gas molecules, such as NO [21–25], CO [23,25], H_2S [26], and SO_2 [27]. Recently, a two-dimensional (2D) graphene porous material, a C_2N monolayer, was successfully prepared via a simple wet chemical reaction [28]. This novel material with a uniform pore distribution has attracted much attention due to its large surface area and good structural stability. Given the uniform cavity structure of C_2N, it has been demonstrated to be a suitable material for anchoring metal atoms. Previous studies have shown that metal-atom-decorated C_2N

monolayers can efficiently trap small gas molecules. For example, Ma et al. proposed 3D transition-metal-modified C_2N as a promising candidate for the low-temperature CO oxidation reaction [29]. Anikina et al. reported that metal-decorated C_2N monolayers have high storage capacities for H_2 [30]. Furthermore, several studies reported that single metal-atom-anchored C_2N monolayers can also act as effective catalysts for N_2 reduction, oxygen reduction, and hydrogen evolution reactions [31–35].

The metal aluminum is environmentally friendly, inexpensive, and abundant in storage. Previous work has shown that decoration with Al atoms can significantly improve the adsorption capacity of 2D materials [36–44]. Specifically, Al-doped graphene showed a good adsorption ability for small molecules, such as N_2O, NO_2, SO_3, and CO_2 [36–40,43]. The Al-embedded C_2N was shown to be a prospective candidate to adsorb and degrade volatile organic compounds, mainly due to a strong electronic transfer between the adsorbed molecules and Al atoms [41,42]. Strong adsorption properties of NO_2 and NH_3 molecules were also observed in Al-MoS_2 [44].

Inspired by these findings, we investigated the reaction mechanism of the NO reduction with CO molecules on an Al-C_2N monolayer based on density functional theory (DFT) calculations. The geometries of reactants, transition states, and products, as well as reaction energies, were calculated in detail. The key intermediates and preferred reaction pathways for NO reduction on Al-C_2N were further identified. The catalytic reactivity of Al-C_2N was also compared with other catalytic materials to evaluate the possibility of using Al-C_2N as a catalyst for NO reduction.

2. Computational Methods

All DFT calculations were carried out at the level of the B3LYP exchange–correlation functional with Grimme's DFT-D3 empirical dispersion correction using the Gaussian09 software package [45–48]. Previous literature confirmed that the B3LYP functional with DFT-D3 is a reasonable condition for calculating intermolecular non-covalent interactions [49]. The 6-31G(d, p) basis set was used to describe all atoms [50]. A pristine C_2N cluster model in this study contained 37 carbon atoms, 12 nitrogen atoms, and 12 hydrogen atoms. All the energies were corrected with zero-point vibrational energy (ZPE). Vibration frequency calculations were performed to verify the optimized structure, where the minimum structure had no imaginary frequency, and the transition state only had one imaginary frequency. Intrinsic reaction coordinate (IRC) calculations were used to verify the transition states [51–53]. Atomic charges were discussed with the natural bond orbital (NBO) analysis [54]. Electron density difference (EDD) plots were obtained with the Multiwfn program [55]. For each adsorption configuration, the EDD plots were calculated as:

$$\Delta\rho = \rho_{A/S} - \rho_A - \rho_S \quad (1)$$

where $\rho_{A/S}$, ρ_A, and ρ_S are the electron density of the total complexes, isolated substrate, and isolated adsorbate, respectively.

The adsorption energy (E_{ads}) of a given adsorbate was defined as:

$$E_{ads} = E_{total} - E_A - E_S \quad (2)$$

where E_{total}, E_A, and E_S are the energies of the total adsorbate-substrate systems, isolated adsorbate, and isolated substrate, respectively.

The change in Gibbs free energy (ΔG) was defined as:

$$\Delta G = \Delta H - T\Delta S \quad (3)$$

where ΔH and ΔS represent the enthalpy with a zero-point energy correction and the entropy change at 298.15 K, respectively.

3. Results and Discussion

3.1. Geometrical Structures and Stability of Pristine C_2N and Al-C_2N Monolayer

Firstly, we examined the geometric structure and stability of the designed Al-C_2N. The optimized structure of the pristine C_2N cluster is shown in Figure 1a. The calculated lattice parameter of 8.286 Å was consistent with the experiment result (8.30 Å) [28]. Then, a single Al atom was attached to the C_2N cluster via two adjacent N atoms (shown in Figure 1b), with both bond lengths being 1.939 Å, in which the Al atom was more preferably anchored at the corners of the six-fold cavity of the C_2N. The calculated bond length value was in line with the previously periodic system-reported results (1.96 Å) [56]. EDD plots revealed a sizeable interaction area between the Al atom and its two adjacent N atoms. It is worth mentioning that the modification of the Al atoms could effectively change the surface properties of the C_2N monolayer. As shown in Figure 1c,d, the uniformly distributed charge on the C_2N monolayer changed to a directional concentrated distribution, which was essential for the subsequent adsorption of gas molecules.

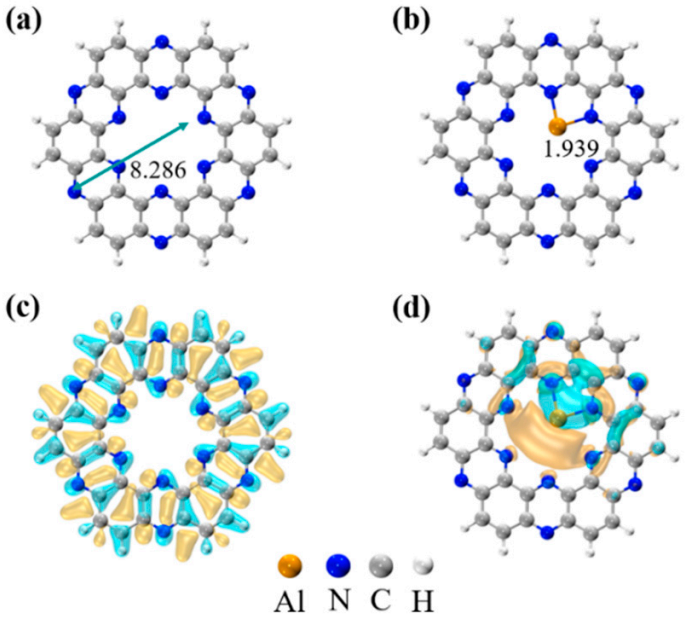

Figure 1. Optimized structures of the (**a**) pristine C_2N cluster and (**b**) Al-C_2N monolayer, respectively. Electron density difference plots (in 0.002 au) for (**c**) pristine C_2N and (**d**) Al-C_2N, respectively. Blue and yellow parts represent charge accumulation and depletion, respectively. All bond lengths are in Å.

To evaluate the thermal stability of the designed Al-C_2N systems, we carried out MD simulations at 300 K and 500 K for 8 ps with a time step of 2 fs under the NVT ensemble (see Figure S1 in the Supplementary Materials). According to the MD simulations, the energies of the Al-C_2N system fluctuated gently, suggesting its high thermodynamic stability.

3.2. Adsorption Behavior of NO and CO Molecules on Al-C_2N Surface

The stable configurations of CO and NO adsorbed on the Al-C_2N surface are displayed in Figure 2. Table 1 summarizes the corresponding adsorption parameters for the NO and CO molecules, including the E_{ads}, ΔG, and charge transfer values. Note that all the calculated ΔG values of the CO or NO molecules adsorbed on the Al-C_2N surface were negative, suggesting that the adsorption of these species was thermodynamically spontaneous.

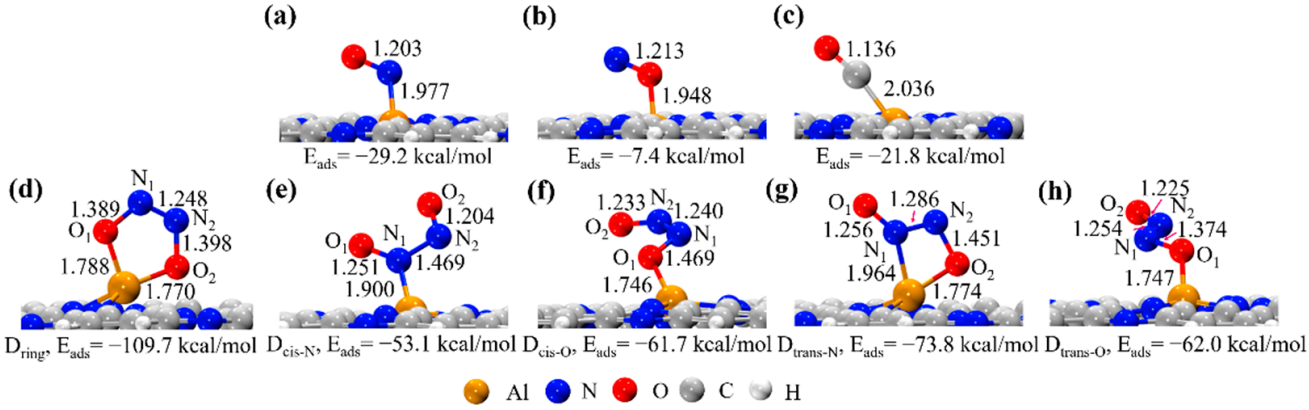

Figure 2. Optimized adsorption configurations for the (**a**) NO (N-end), (**b**) NO (O-end), (**c**) CO, (**d**) ring-$(NO)_2$ dimers, (**e**) cis-$(NO)_2$ dimers (N-end), (**f**) cis-$(NO)_2$ dimers (O-end), (**g**) trans-$(NO)_2$ dimers (N-end), and (**h**) trans-$(NO)_2$ dimers (O-end) on Al-C_2N surface. All bond lengths are in Å.

Table 1. Calculated adsorption energies (E_{ads}, kcal/mol), adsorption free energies (ΔG, kcal/mol), and net charge-transfer values (q, e) for different adsorption species on the Al-C_2N surface, along with the corresponding energy barriers (E_a, kcal/mol) and reaction energies (ΔE_r) for a single NO or $(NO)_2$ dimer reduction on Al-C_2N surface.

Adsorbate	E_{ads}	ΔG	q [1]	E_a	Path	ΔE_r
CO	−21.8	−11.4	0.083	-	-	-
NO (O-end)	−7.4	−4.1	−0.337	-	-	-
NO (N-end)	−29.2	−17.8	−0.430	68.0	-	41.1
D_{ring}	−109.7	−86.3	−1.377	33.5 (43.1)	Ia (Ib)	23.2 (−67.7)
D_{cis-N}	−53.1	−31.8	−0.672	3.6	II	−8.6
D_{cis-O}	−61.7	−39.9	−0.731	2.7	II	−24.8
$D_{trans-N}$	−73.8	−52.3	−1.303	16.5	III	−12.7
$D_{trans-O}$	−62.0	−40.0	−0697	12.7	IV	−24.5

[1] Positive and negative values of q correspond to the net charge transfer from the adsorbate to the Al-C_2N and the net charge transfer from the Al-C_2N surface to the adsorbate, respectively.

The adsorption geometries of the NO, CO, and $(NO)_2$ dimers on Al-C_2N are shown in Figure 2. For the NO molecules, two possible adsorption modes (including N-end and O-end) were investigated. From Figure 2a,b, it can be seen that the NO molecules were tilted concerning the Al-C_2N surface, consistent with previous reports [24,57,58]. As evident, the calculated N-O bond lengths of the NO molecules were elongated to 1.203 Å and 1.213 Å, respectively, when compared with the free NO molecule (1.160 Å). The E_{ads} values for the N-end and O-end adsorption modes were −29.2 and −7.4 kcal/mol, respectively, which was more negative than the values in Si-doped graphene (−18.4 and −4.4 kcal/mol) [57]. From the viewpoint of adsorption energy, it is clear that the N-end adsorption was energetically more favorable than the O-end. This result was also supported by the NBO charge analysis, in which the N-end mode was accompanied by a larger charge transfer of 0.430 e from the Al-C_2N surface to the $2\pi^*$ orbital of the NO molecule (Table 1).

As for the CO molecules, our results demonstrated that CO preferred to adsorb on the Al-C_2N surface via its C-end. Figure 2c demonstrates that the C-O bond length of CO was nearly unchanged compared to that of the free CO molecule (1.14 Å), indicating that CO was not activated after being adsorbed on the Al-C_2N surface. Based on the E_{ads} value, the adsorption of CO (−21.8 kcal/mol) on Al-C_2N was weaker than that of NO (−29.2 kcal/mol). In this case, it was expected that the tendency of the NO molecule to adsorb onto the Al-C_2N surface was greater than that of CO. Unlike the NO molecules, CO acted as the electron donor, where the charge value transferred from the CO molecule to the Al-C_2N surface was 0.083 e (Table 1).

Next, we considered the $(NO)_2$ dimer configuration formed by two NO molecules co-adsorbed on the Al-C_2N surface. The $(NO)_2$ dimer was characterized for the first time by Dinerman and Ewing using infrared spectroscopy [59]. The stable $(NO)_2$ dimer adsorption configurations are illustrated in Figure 2d–h. The IR spectra plots of five $(NO)_2$ dimers on the Al-C_2N surface are displayed in Figure S2. As can be seen, five different $(NO)_2$ dimers were obtained on the Al-C_2N surface.

Figure 2d shows a five-membered ring $(NO)_2$ dimer structure (labeled as D_{ring}), in which both NO molecules were bound to the Al site through their O-end. The bond lengths of the two formed Al-O bonds and the N_1-N_2 bond were 1.788, 1.770, and 1.248 Å, respectively. This structure was similar to that of Si-doped graphene (1.783, 1.762, and 1.240 Å for two Si-O bonds and the N_1-N_2 bond) [60]. Figure 2e,g display the cis- and trans-$(NO)_2$ dimer structures at the N-end (labeled as $D_{cis\text{-}N}$ and $D_{trans\text{-}N}$), respectively, in which one NO molecule was adsorbed into the Al site via its N-end and two NO molecules were bound through N-N bonds. The calculated bond lengths of the N_1-N_2 bond were 1.469 and 1.286 Å, respectively. It is noteworthy that two novel $(NO)_2$ dimer structures were explored in this work, which have not been reported in current catalysts [57,59,61–64]. Figure 2f,h correspond to two novel cis- and trans-$(NO)_2$ dimer structures at the O-end (labeled as $D_{cis\text{-}O}$ and $D_{trans\text{-}O}$) with N_1-N_2 bond lengths of 1.240 and 1.254 Å, respectively. Among the above $(NO)_2$ dimers, the calculated N_1-N_2 bond lengths ranged from 1.505 to 1.233 Å, which were much shorter than the value in the gas phase $(NO)_2$ dimer (1.970 Å). As shown in Table 1, the calculated adsorption energies of the five $(NO)_2$ dimers on the Al-C_2N surface were significantly enhanced, with values of −109.7, −53.1, −61.7, −73.8, and −62.0 kcal/mol, respectively, which were larger than twice that of a NO molecule (−29.2 kcal/mol). This indicated that the addition of the second NO molecule was beneficial for strengthening the interaction between the catalyst and NO molecule. Similar results were further verified with the NBO charge analysis, where the considerable charge-transfer values from the Al-C_2N surface to $(NO)_2$ dimers were −1.377, −0.672, −0.731, −1.303, and −0697, respectively (Table 1).

3.3. NO Reduction Mechanism on Al-C_2N Surface

Here, the NO reduction mechanism mainly included the direct decomposition process and the $(NO)_2$ dimer reduction process. For the former, a NO molecule was directly decomposed into O and N atoms. For the latter, two NO molecules were co-adsorbed forming $(NO)_2$ dimers, followed by their decomposition into N_2O molecules and O atoms. Subsequently, the N_2O molecules were desorbed, and the remaining O atoms could be removed with the NO or CO molecules.

3.3.1. NO Direct Decomposition Process

Figure 3 shows the energy profile of the NO direct decomposition process on Al-C_2N, where the energy sum of Al-C_2N and free NO molecules was set as the reference energy. As seen, the reaction began with the NO molecule adsorbed on Al-C_2N via its N-end. In the TS structure, the calculated O-N bond length of the NO molecule was elongated from 1.215 Å to 2.420 Å. In the FS structure, the O-N bond was broken and the distance between the O and N atoms was 3.292 Å. Our results showed that the NO direct decomposition process was unfavorable both in kinetics and thermodynamics due to the high reaction energy barrier (68.0 kcal/mol) and endothermic nature (41.1 kcal/mol), which agreed withprevious reports, such as Si-doped graphene (39.2 kcal/mol) [24], Si-doped BN nanosheets (57.9 kcal/mol) [60], and Fe-doped graphene (124.1 kcal/mol) [25].

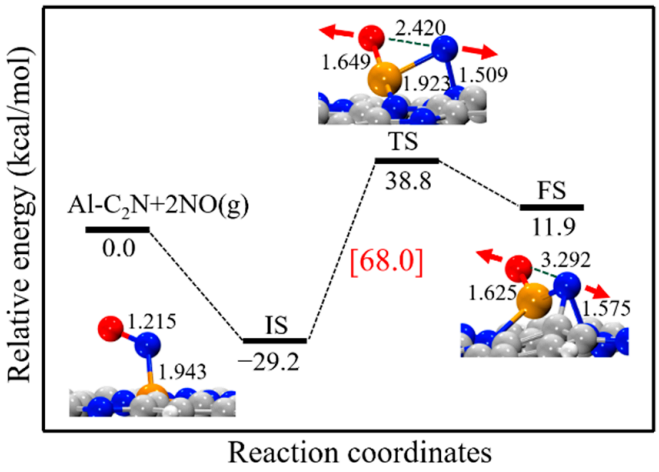

Figure 3. The energy profile and corresponding structure for the NO direct decomposition process on Al-C_2N. All bond lengths are in Å.

3.3.2. $(NO)_2$ Dimer Reduction Process

In this section, we examined the possible reaction pathways of the $(NO)_2$ dimer reduction process on Al-C_2N. There were four reaction pathways starting with different $(NO)_2$ dimer structures described as path I, path II, path III, and path IV, respectively. For simplicity, the remaining oxygen atoms on the Al-C_2N surface were labeled as O_{ads}.

In path Ia, the five-membered ring $(NO)_2$ dimer structure (D_{ring}) was the initial state. The energy profile and corresponding minima state and transition state are displayed in Figure 4a. As can be seen, the D_{ring} structure could be decomposed into the product (N_2O + O_{ads}) through the transition state with a high-energy barrier of 33.5 kcal/mol. In the TS structure, the N_2-O_2 bond broke with the bond length increasing from 1.398 to 2.364 Å, while the N_1-N_2 bond length decreased from 1.248 to 1.141 Å. The entire process from D_{ring} to the FS structure was endothermic by 23.2 kcal/mol. Given the high reaction barrier and endothermicity, it was expected that the D_{ring} dimer reduction on Al-C_2N was unfavorable both kinetically and thermodynamically.

In path Ib, a two-step reaction was identified: (i) $(NO)_2 \rightarrow N_2 + 2O_{ads}$, followed by (ii) $CO + O_{ads} \rightarrow CO_2$. As shown in Figure 4b, the D_{ring} structure was taken as the initial state and, subsequently, CO was physisorbed over Al-C_2N to form an intermediate state (the MS1 structure). In the TS1 structure, two N-O bonds broke with the bond lengths increasing to 1.880 and 1.978 Å, respectively, while the N_1-N_2 bond length was shortened to 1.144 Å. Next, N_2 was completely formed in the MS2 structure. In the next step, CO approached the O_1 atom. The $O_1 \cdots C$ bond's length reduced from 2.859 to 2.152 Å and, finally, formed the CO_2 molecule. Note that the energy barriers of the first and second steps were 43.1 and 1.6 kcal/mol, respectively, which could be provided by the larger exothermic reaction energy (−67.7 kcal/mol, from D_{ring} to FS).

In path II, the reaction started with the co-adsorption of two NO molecules to generate a cis-$(NO)_2$ dimer (N-end, $D_{cis\text{-}N}$) structure, as shown in Figure 5. As seen, this step had a negligible energy barrier and was exothermic by 17.3 kcal/mol. Then, the $D_{cis\text{-}N}$ structure could be converted to the more stable cis-$(NO)_2$ dimer (O-end, $D_{cis\text{-}O}$) structure by overcoming a small energy barrier of 3.6 kcal/mol, being exothermic by 8.6 kcal/mol. Finally, the $D_{cis\text{-}O}$ structure decomposed into the product (N_2O and O_{ads} species) through TS2 by breaking the N_1-O1 bond. In the TS2 structure, the N_1-O_1 distance significantly elongated from 1.469 to 1.659 Å, while the N_1-N_2 distance decreased from 1.240 to 1.207 Å. We note that there was a negligible energy barrier for this step (2.7 kcal/mol), which was exothermic by 24.8 kcal/mol. Since the entire reaction was a highly exothermic process (−50.7 kcal/mol, from IS to FS), it was thermodynamically feasible under mild conditions.

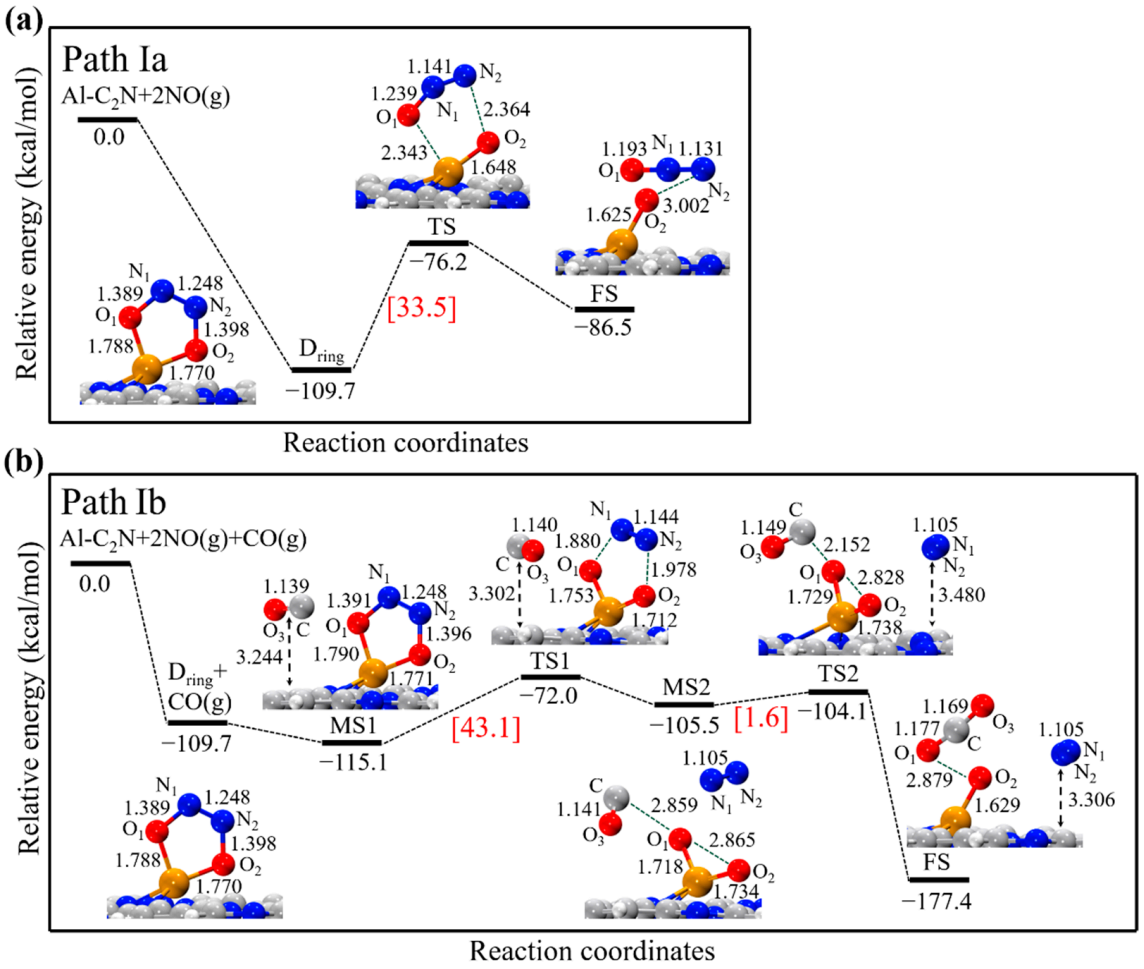

Figure 4. The energy profile and corresponding structure of the D_{ring} dimer reduction process on Al-C_2N; (**a**) $(NO)_2 \rightarrow N_2O + O_{ads}$ (path Ia), (**b**) $(NO)_2 + CO \rightarrow N_2 + CO_2 + O_{ads}$ (path Ib). All bond lengths are in Å.

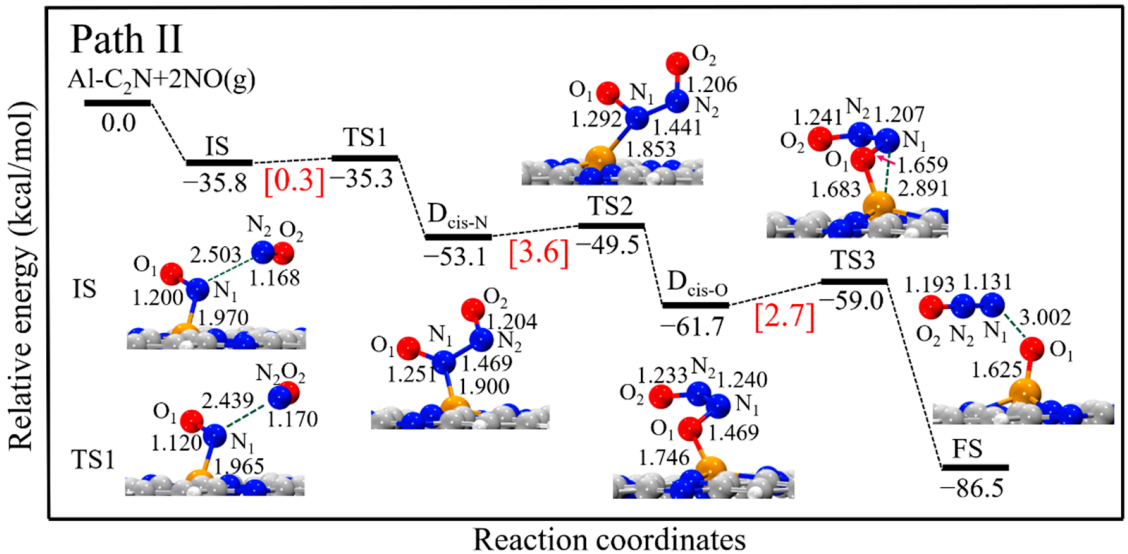

Figure 5. The energy profiles and corresponding structures of the $D_{cis\text{-}N}$ and $D_{cis\text{-}O}$ dimer reduction process on Al-C_2N. All bond lengths are in Å.

In path III, the trans-$(NO)_2$ dimer structure (N-end, $D_{trans\text{-}N}$) was considered the starting point for the NO reduction on Al-C_2N. From Figure 6a, one could see that the NO molecule bonded with the Al site through the N-end, whereas another NO molecule was weakly physisorbed on the surface, with the distance between the N_1 and N_2 atoms being 2.445 Å. The co-adsorption energy of 2NO was −35.6 kcal/mol. Next, the $D_{trans\text{-}N}$ structure was formed through a barrierless process. In this structure, the calculated N_1-N_2 bond was shortened to 1.286 Å, while the N_2-O_2 bond was extended to 1.451 Å. In the TS structure, the N_2-O_2 bond was significantly extended from 1.451 to 2.604 Å. Finally, the N_2-O_2 bond was completely broken, forming N_2O and O_{ads} moieties. This path revealed a high reaction barrier of 16.5 kcal/mol and was exothermic by 12.7 kcal/mol. Figure 6b exhibits path IV, starting from the trans-$(NO)_2$ dimer structure (O-end, $D_{trans\text{-}O}$). In this path, 2NO molecules formed the $D_{trans\text{-}O}$ structure through an extremely low-energy barrier (1.6 kcal/mol). Then, the N_1-O_1 bond length was significantly extended from 1.374 Å in the $D_{trans\text{-}O}$ structure to 1.696 Å in the TS2 structure. The energy barrier for this step was 12.7 kcal/mol, which could be provided by the exothermic reaction energy (−24.5 kcal/mol).

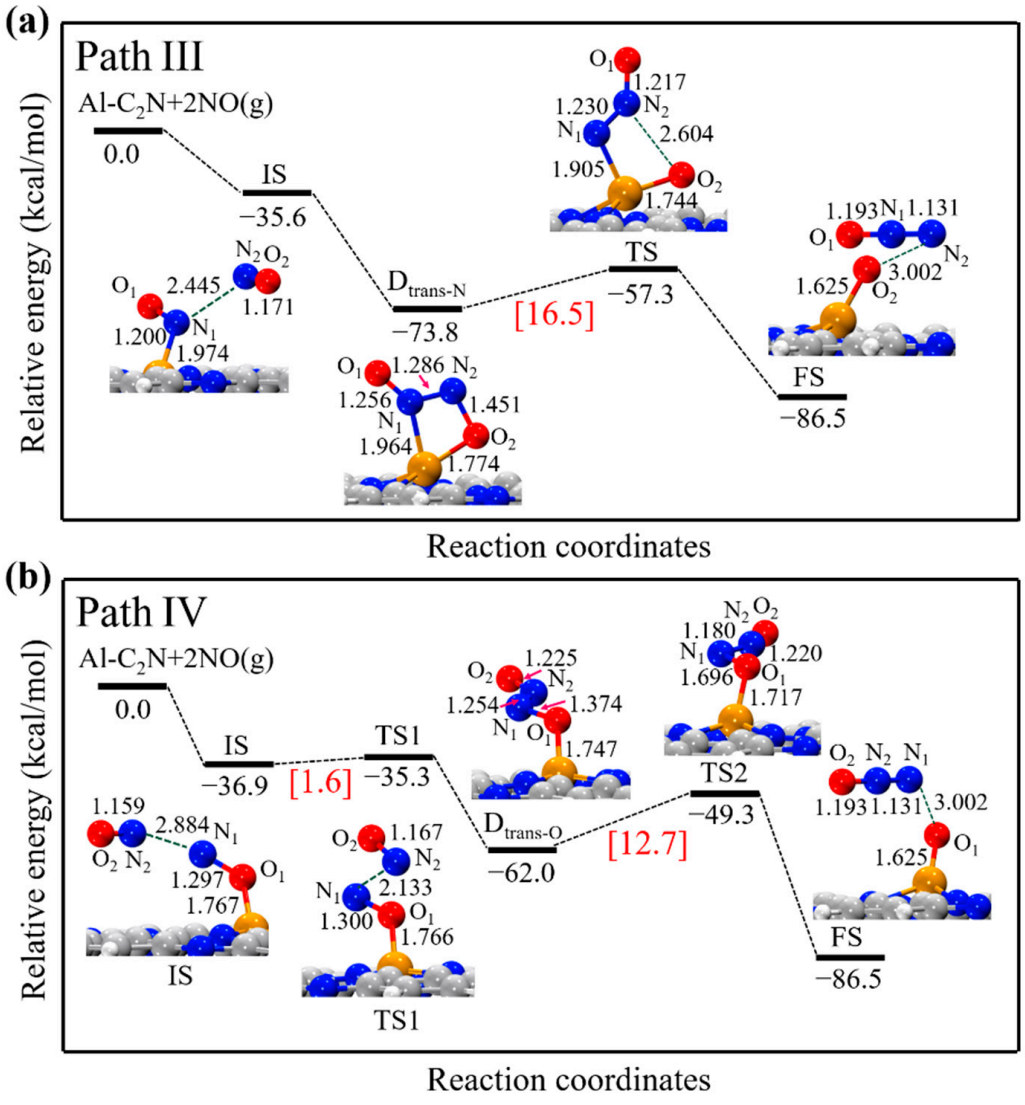

Figure 6. The energy profiles and corresponding structures of the (**a**) $D_{trans\text{-}N}$ and (**b**) $D_{trans\text{-}O}$ dimer reduction process on Al-C_2N. All bond lengths are in Å.

According to our results, it was found that the NO reduction preferred to proceed via the $(NO)_2$ dimer reduction process. First, the E_{ads} values of the $(NO)_2$ dimers were much larger than that of the single NO molecule. Second, the $(NO)_2$ dimer reduction process

was thermodynamically and kinetically more favorable than the NO direct decomposition process. Based on the energy barriers (E_a) and reaction energies (ΔE_r), the NO dimer reduction on the Al-C_2N surface could occur via path II and path IV (Table 1). Path II was energetically the most favorable pathway with the max energy barrier for the $(NO)_2 \rightarrow N_2O + O_{ads}$ reaction of only 3.6 kcal/mol, which was even smaller than the values in noble metal catalysts, such as Pd-BNNS (14.9 kcal/mol) [58], Au (8.1 kcal/mol) [65], and Ag (6.2 kcal/mol) [66]. These results implied that the Al-C_2N catalyst exhibited good catalytic activity towards the NO reduction.

After the N_2O desorption, the remaining O_{ads} atom could be removed with the NO or CO molecules. In our previous work, we revealed that Al-C_2N could serve as a promising catalyst for N_2O reduction to environmentally friendly N_2 molecules [67]. Figure 7 shows the reaction pathways of $O_{ads} + NO \rightarrow NO_2$ and $O_{ads} + CO \rightarrow CO_2$ on Al-C_2N, respectively. Our results showed that $O_{ads} + NO \rightarrow NO_2$ was an endothermic process (7.5 kcal/mol), and quite a high-energy barrier (15.5 kcal/mol) required to be surmounted. As seen in Figure 7b, the $O_{ads} + CO \rightarrow CO_2$ reaction was an exothermic process, and an energy barrier of only 6.6 kcal/mol was needed for Al-C_2N, which was smaller than the value for Pt-graphene (13.4 kcal/mol) [68]. This meant that CO_2 molecules were more likely to form on the Al-C_2N catalyst in the existence of NO molecules.

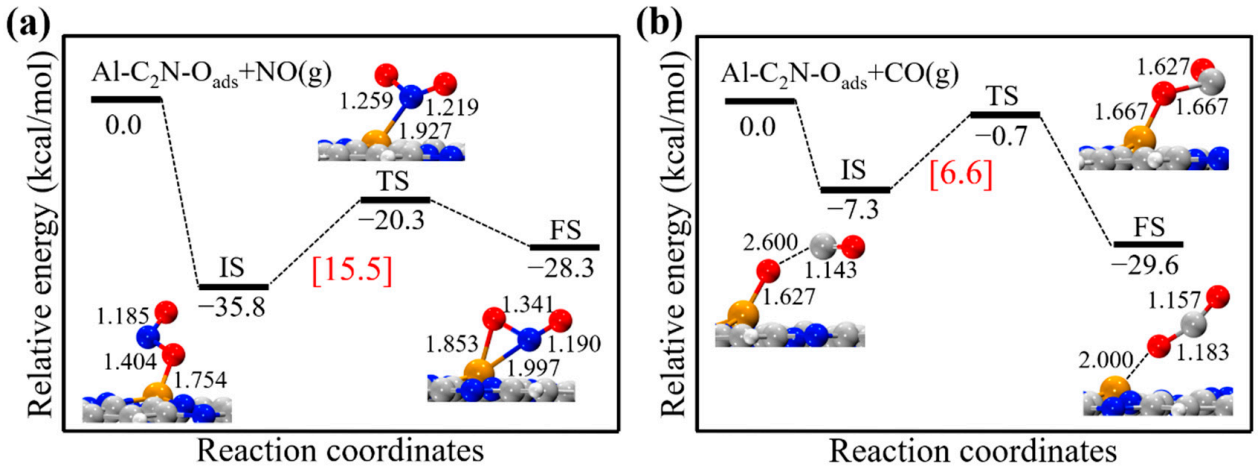

Figure 7. The energy profiles and corresponding structures for the step of (**a**) $O_{ads} + NO \rightarrow NO_2$ and (**b**) $O_{ads} + CO \rightarrow CO_2$ on Al-C_2N, respectively. All bond lengths are in Å.

4. Conclusions

In this work, we investigated the NO reduction over low-cost Al-C_2N catalysts using DFT calculations in detail. According to the adsorption energy and charge transfer values, the adsorption of NO on the catalyst was significantly stronger than that of CO, which suggested that the Al-C_2N catalyst was more selective to NO than CO. For the NO reduction mechanism, our results showed that the NO direct decomposition process was barely possible due to the extremely high-energy barrier and endothermicity. In contrast, the catalysis of the NO reduction via the $(NO)_2$ dimer reduction process was both thermodynamically and kinetically favorable. It was found that cis-$(NO)_2$ dimer structures were key intermediates for the NO reduction, where the calculated max barriers along the most energetically favorable pathway (path II) was only 3.6 kcal/mol. The remaining O_{ads} species on Al-C_2N could be eliminated with CO molecules, which required overcoming the energy barriers of only 6.6 kcal/mol. Overall, Al-C_2N is expected to be a promising catalyst for NO reduction with CO.

Supplementary Materials: The following supporting information can be downloaded at: https://www.mdpi.com/article/10.3390/molecules27185790/s1. Figure S1: molecular dynamics simulation for Al-C_2N catalyst at (a) 300 K and (b) 500 K, respectively; Figure S2: IR spectra plots for five kinds of $(NO)_2$ dimers on the Al-C_2N surface.

Author Contributions: Conceptualization, methodology, software, and writing original draft, X.L.; investigation, software, and data curation, Y.X.; conceptualization, supervision, and writing—review and editing, L.S. All authors have read and agreed to the published version of the manuscript.

Funding: This research received no external funding.

Institutional Review Board Statement: Not applicable.

Informed Consent Statement: Not applicable.

Data Availability Statement: All data presented in this study are available in this published article and Supplementary Materials.

Conflicts of Interest: The authors declare no conflict of interest.

Sample Availability: Samples of the compounds are not available from the authors.

References

1. Liu, Z.S.; Yu, F.; Ma, C.H.; Dan, J.M.; Luo, J.; Dai, B. A Critical Review of Recent Progress and Perspective in Practical Denitration Application. *Catalysts* **2019**, *9*, 771. [CrossRef]
2. Seitzinger, S.P.; Phillips, L. Nitrogen stewardship in the Anthropocene. *Science* **2017**, *357*, 350–351. [CrossRef]
3. Janssens, T.V.W.; Vennestrom, P.N.R. A molecular dance to cleaner air. *Science* **2017**, *357*, 866–867. [CrossRef] [PubMed]
4. Gholami, Z.; Luo, G.H.; Gholami, F.; Yang, F. Recent advances in selective catalytic reduction of NO_x by carbon monoxide for flue gas cleaning process: A review. *Catal. Rev.-Sci. Eng.* **2021**, *63*, 68–119. [CrossRef]
5. Toyao, T.; Jing, Y.; Kon, K.; Hayama, T.; Nagaoka, S.; Shimizu, K.-i. Catalytic NO–CO Reactions over La-Al_2O_3 Supported Pd: Promotion Effect of La. *Chem. Lett.* **2018**, *47*, 1036–1039. [CrossRef]
6. Tou, A.; Einaga, H.; Teraoka, Y. Effect of co-deposition of $LaFeO_3$ on the catalytic properties of Pd on Al_2O_3 support for CO–O_2 and NO–CO reactions. *React. Kinet. Mech. Catal.* **2015**, *114*, 409–420. [CrossRef]
7. Liu, K.J.; Yu, Q.B.; Liu, J.L.; Wang, K.; Han, Z.C.; Xuan, Y.N.; Qin, Q. Selection of catalytically active elements for removing NO and CO from flue gas at low temperatures. *New J. Chem.* **2017**, *41*, 13993–13999. [CrossRef]
8. Grigorkina, G.S.; Ramonova, A.G.; Kibizov, D.D.; Fukutani, K.; Magkoev, T.T. Interaction of CO, NO, and H_2 molecules on the surface of a Ni/MgO(111) metal oxide system. *Tech. Phys. Lett.* **2017**, *43*, 611–614. [CrossRef]
9. Song, J.; Wang, Z.; Cheng, X.; Wang, X. State-of-Art Review of NO Reduction Technologies by CO, CH_4 and H_2. *Processes* **2021**, *9*, 563. [CrossRef]
10. Kravchenko, P.; Krishnan, V.; Hibbitts, D. Mechanism and Effects of Coverage and Particle Morphology on Rh-Catalyzed NO–H_2 Reactions. *J. Phys. Chem. C* **2020**, *124*, 13291–13303. [CrossRef]
11. Hibbitts, D.D.; Jiménez, R.; Yoshimura, M.; Weiss, B.; Iglesia, E. Catalytic NO activation and NO–H_2 reaction pathways. *J. Catal.* **2014**, *319*, 95–109. [CrossRef]
12. Sun, X.; Guo, R.T.; Liu, S.W.; Liu, J.; Pan, W.G.; Shi, X.; Qin, H.; Wang, Z.Y.; Qiu, Z.Z.; Liu, X.Y. The promoted performance of CeO_2 catalyst for NH_3-SCR reaction by NH_3 treatment. *Appl. Surf. Sci.* **2018**, *462*, 187–193. [CrossRef]
13. Wang, Y.X.; Kapteijn, F.; Makkee, M. NO_x reduction in the Di-Air system over noble metal promoted ceria. *Appl. Catal. B-Environ.* **2018**, *231*, 200–212. [CrossRef]
14. Karmaoui, M.; Lajaunie, L.; Tobaldi, D.M.; Leonardi, G.; Benbayer, C.; Arenal, R.; Labrincha, J.A.; Neri, G. Modification of anatase using noble-metals (Au, Pt, Ag): Toward a nanoheterojunction exhibiting simultaneously photocatalytic activity and plasmonic gas sensing. *Appl. Catal. B-Environ.* **2017**, *218*, 370–384. [CrossRef]
15. Yao, Y.; Zhu, S.; Wang, H.; Li, H.; Shao, M. A Spectroscopic Study on the Nitrogen Electrochemical Reduction Reaction on Gold and Platinum Surfaces. *J. Am. Chem. Soc.* **2018**, *140*, 1496–1501. [CrossRef] [PubMed]
16. Huai, L.-Y.; He, C.-Z.; Wang, H.; Wen, H.; Yi, W.-C.; Liu, J.-Y. NO dissociation and reduction by H_2 on Pd(1 1 1): A first-principles study. *J. Catal.* **2015**, *322*, 73–83. [CrossRef]
17. Lin, J.; Wang, A.; Qiao, B.; Liu, X.; Yang, X.; Wang, X.; Liang, J.; Li, J.; Liu, J.; Zhang, T. Remarkable performance of Ir_1/FeO_x single-atom catalyst in water gas shift reaction. *J. Am. Chem. Soc.* **2013**, *135*, 15314–15317. [CrossRef]
18. Zhong, W.; Qiu, Y.; Shen, H.; Wang, X.; Yuan, J.; Jia, C.; Bi, S.; Jiang, J. Electronic Spin Moment As a Catalytic Descriptor for Fe Single-Atom Catalysts Supported on C_2N. *J. Am. Chem. Soc.* **2021**, *143*, 4405–4413. [CrossRef]
19. Luo, M.; Liang, Z.; Liu, C.; Qi, X.; Chen, M.; Ur Rehman Sagar, R.; Yang, H.; Liang, T. Single–atom manganese and nitrogen co-doped graphene as low-cost catalysts for the efficient CO oxidation at room temperature. *Appl. Surf. Sci.* **2021**, *536*, 147809. [CrossRef]

20. Wei, H.; Liu, X.; Wang, A.; Zhang, L.; Qiao, B.; Yang, X.; Huang, Y.; Miao, S.; Liu, J.; Zhang, T. FeO_x-supported platinum single-atom and pseudo-single-atom catalysts for chemoselective hydrogenation of functionalized nitroarenes. *Nat. Commun.* **2014**, *5*, 5634. [CrossRef] [PubMed]
21. Mudchimo, T.; Namuangruk, S.; Kungwan, N.; Jungsuttiwong, S. Carbon-doped boron nitride nanosheet as a promising metal-free catalyst for NO reduction: DFT mechanistic study. *Appl. Catal. A Gen.* **2018**, *557*, 79–88. [CrossRef]
22. Esrafili, M.D.; Asadollahi, S.; Heydari, S. A DFT study on NO reduction to N_2O using Al- and P-doped hexagonal boron nitride nanosheets. *J. Mol. Graph. Model.* **2019**, *89*, 41–49. [CrossRef]
23. Chu, M.; Liu, X.; Sui, Y.; Luo, J.; Meng, C. Unique Reactivity of Transition Metal Atoms Embedded in Graphene to CO, NO, O_2 and O Adsorption: A First-Principles Investigation. *Molecules* **2015**, *20*, 19540–19553. [CrossRef] [PubMed]
24. Maitarad, P.; Junkaew, A.; Promarak, V.; Shi, L.Y.; Namuangruk, S. Complete catalytic cycle of NO decomposition on a silicon-doped nitrogen-coordinated graphene: Mechanistic insight from a DFT study. *Appl. Surf. Sci.* **2020**, *508*, 145255. [CrossRef]
25. Hu, L.L.; Zhang, Y.; Zhang, H.; Wu, Y.X. Catalytic reduction of NO by CO over Fe-doped penta-graphene as a promising catalyst: A density functional study. *Mol. Catal.* **2020**, *496*, 111194. [CrossRef]
26. Xie, T.; Wang, P.; Tian, C.; Zhao, G.; Jia, J.; He, C.; Zhao, C.; Wu, H. Adsorption Characteristics of Gas Molecules Adsorbed on Graphene Doped with Mn: A First Principle Study. *Molecules* **2022**, *27*, 2315. [CrossRef] [PubMed]
27. Xie, T.; Wang, P.; Tian, C.; Zhao, G.; Jia, J.; Zhao, C.; Wu, H. The Adsorption Behavior of Gas Molecules on Co/N Co-Doped Graphene. *Molecules* **2021**, *26*, 7700. [CrossRef]
28. Mahmood, J.; Lee, E.K.; Jung, M.; Shin, D.; Jeon, I.Y.; Jung, S.M.; Choi, H.J.; Seo, J.M.; Bae, S.Y.; Sohn, S.D.; et al. Nitrogenated holey two-dimensional structures. *Nat. Commun.* **2015**, *6*, 6486. [CrossRef] [PubMed]
29. Ma, D.W.; Wang, Q.G.; Yan, X.W.; Zhang, X.W.; He, C.Z.; Zhou, D.W.; Tang, Y.A.; Lu, Z.S.; Yang, Z.X. 3d transition metal embedded C_2N monolayers as promising single-atom catalysts: A first-principles study. *Carbon* **2016**, *105*, 463–473. [CrossRef]
30. Anikina, E.; Naqvi, S.R.; Bae, H.; Lee, H.; Luo, W.; Ahuja, R.; Hussain, T. High-capacity reversible hydrogen storage properties of metal-decorated nitrogenated holey graphenes. *Int. J. Hydrog. Energy* **2022**, *47*, 10654–10664. [CrossRef]
31. Chakrabarty, S.; Das, T.; Banerjee, P.; Thapa, R.; Das, G.P. Electron doped C_2N monolayer as efficient noble metal-free catalysts for CO oxidation. *Appl. Surf. Sci.* **2017**, *418*, 92–98. [CrossRef]
32. Mahmood, J.; Li, F.; Kim, C.; Choi, H.J.; Gwon, O.; Jung, S.M.; Seo, J.M.; Cho, S.J.; Ju, Y.W.; Jeong, H.Y.; et al. Fe@C_2N: A highly-efficient indirect-contact oxygen reduction catalyst. *Nano Energy* **2018**, *44*, 304–310. [CrossRef]
33. Li, X.; Cui, P.; Zhong, W.; Li, J.; Wang, X.; Wang, Z.; Jiang, J. Graphitic carbon nitride supported single-atom catalysts for efficient oxygen evolution reaction. *Chem. Commun.* **2016**, *52*, 13233–13236. [CrossRef]
34. Zhang, X.; Chen, A.; Zhang, Z.; Zhou, Z. Double-atom catalysts: Transition metal dimer-anchored C_2N monolayers as N_2 fixation electrocatalysts. *J. Mater. Chem. A* **2018**, *6*, 18599–18604. [CrossRef]
35. Wang, Z.; Yu, Z.; Zhao, J. Computational screening of a single transition metal atom supported on the C_2N monolayer for electrochemical ammonia synthesis. *Phys. Chem. Chem. Phys.* **2018**, *20*, 12835–12844. [CrossRef] [PubMed]
36. Lv, Y.A.; Zhuang, G.L.; Wang, J.G.; Jia, Y.B.; Xie, Q. Enhanced role of Al or Ga-doped graphene on the adsorption and dissociation of N_2O under electric field. *Phys. Chem. Chem. Phys.* **2011**, *13*, 12472–12477. [CrossRef]
37. Esrafili, M.D.; Saeidi, N.; Nematollahi, P. A DFT study on SO_3 capture and activation over Si- or Al-doped graphene. *Chem. Phys. Lett.* **2016**, *658*, 146–151. [CrossRef]
38. Peyghan, A.A.; Noei, M.; Tabar, M.B. A large gap opening of graphene induced by the adsorption of CO on the Al-doped site. *J. Mol. Model.* **2013**, *19*, 3007–3014. [CrossRef]
39. Ao, Z.M.; Li, S.; Jiang, Q. Correlation of the applied electrical field and CO adsorption/desorption behavior on Al-doped graphene. *Solid State Commun.* **2010**, *150*, 680–683. [CrossRef]
40. Rad, A.S. First principles study of Al-doped graphene as nanostructure adsorbent for NO_2 and N_2O: DFT calculations. *Appl. Surf. Sci.* **2015**, *357*, 1217–1224. [CrossRef]
41. Su, Y.T.; Li, W.L.; Li, G.Y.; Ao, Z.M.; An, T.C. Density functional theory investigation of the enhanced adsorption mechanism and potential catalytic activity for formaldehyde degradation on Al-decorated C_2N monolayer. *Chin. J. Catal.* **2019**, *40*, 664–672. [CrossRef]
42. Su, Y.T.; Ao, Z.M.; Ji, Y.M.; Li, G.Y.; An, T.C. Adsorption mechanisms of different volatile organic compounds onto pristine C_2N and Al-doped C_2N monolayer: A DFT investigation. *Appl. Surf. Sci.* **2018**, *450*, 484–491. [CrossRef]
43. Shokuhi Rad, A.; Pouralijan Foukolaei, V. Density functional study of Al-doped graphene nanostructure towards adsorption of CO, CO_2 and H_2O. *Synth. Met.* **2015**, *210*, 171–178. [CrossRef]
44. Luo, H.; Cao, Y.J.; Zhou, J.; Feng, J.M.; Cao, J.M.; Guo, H. Adsorption of NO_2, NH_3 on monolayer MoS_2 doped with Al, Si, and P: A first-principles study. *Chem. Phys. Lett.* **2016**, *643*, 27–33. [CrossRef]
45. Frisch, M.J.; Trucks, G.W.; Schlegel, H.B.; Scuseria, G.E.; Robb, M.A.; Cheeseman, J.R.; Scalmani, G.; Barone, V.; Mennucci, B.; Petersson, G.A.; et al. *Gaussian 09*; Gaussian, Inc.: Wallingford, CT, USA, 2009.
46. Becke, A.D. Density-functional exchange-energy approximation with correct asymptotic behavior. *Phys. Rev. A* **1988**, *38*, 3098–3100. [CrossRef]
47. Grimme, S.; Antony, J.; Ehrlich, S.; Krieg, H. A consistent and accurate ab initio parametrization of density functional dispersion correction (DFT-D) for the 94 elements H-Pu. *J. Chem. Phys.* **2010**, *132*, 154104. [CrossRef] [PubMed]

48. Lee, C.; Yang, W.; Parr, R.G. Development of the Colle-Salvetti correlation-energy formula into a functional of the electron density. *Phys. Rev. B: Condens. Matter* **1988**, *37*, 785–789. [CrossRef]
49. Witte, J.; Goldey, M.; Neaton, J.B.; Head-Gordon, M. Beyond Energies: Geometries of Nonbonded Molecular Complexes as Metrics for Assessing Electronic Structure Approaches. *J. Chem. Theory Comput.* **2015**, *11*, 1481–1492. [CrossRef] [PubMed]
50. Ditchfield, R.; Hehre, W.J.; Pople, J.A. Self-Consistent Molecular-Orbital Methods. IX. An Extended Gaussian-Type Basis for Molecular-Orbital Studies of Organic Molecules. *J. Chem. Phys.* **1971**, *54*, 724–728. [CrossRef]
51. Fukui, K. Formulation of the reaction coordinate. *J. Phys. Chem.* **2002**, *74*, 4161–4163. [CrossRef]
52. Fukui, K. The path of chemical reactions—The IRC approach. *Acc. Chem. Res.* **2002**, *14*, 363–368. [CrossRef]
53. Gonzalez, C.; Schlegel, H.B. Reaction path following in mass-weighted internal coordinates. *J. Phys. Chem.* **2002**, *94*, 5523–5527. [CrossRef]
54. Reed, A.E.; Curtiss, L.A.; Weinhold, F. Intermolecular interactions from a natural bond orbital, donor-acceptor viewpoint. *Chem. Rev.* **2002**, *88*, 899–926. [CrossRef]
55. Lu, T.; Chen, F. Multiwfn: A multifunctional wavefunction analyzer. *J. Comput. Chem.* **2012**, *33*, 580–592. [CrossRef] [PubMed]
56. Zhang, Y.; Mo, Y.; Cao, Z. Rational Design of Main Group Metal-Embedded Nitrogen-Doped Carbon Materials as Frustrated Lewis Pair Catalysts for CO_2 Hydrogenation to Formic Acid. *ACS Appl. Mater. Interfaces* **2022**, *14*, 1002–1014. [CrossRef]
57. Chen, Y.; Liu, Y.J.; Wang, H.X.; Zhao, J.X.; Cai, Q.H.; Wang, X.Z.; Ding, Y.H. Silicon-doped graphene: An effective and metal-free catalyst for NO reduction to N_2O? *ACS Appl. Mater. Interfaces* **2013**, *5*, 5994–6000. [CrossRef]
58. Esrafili, M.D.; Heydari, S.; Dinparast, L. A comparative DFT study about surface reactivity and catalytic activity of Pd- and Ni-doped BN nanosheets: NO reduction by CO molecule. *Struct. Chem.* **2019**, *30*, 1647–1657. [CrossRef]
59. Dinerman, C.E.; Ewing, G.E. Infrared Spectrum, Structure, and Heat of Formation of Gaseous $(NO)_2$. *J. Chem. Phys.* **1970**, *53*, 626–631. [CrossRef]
60. Esrafili, M.D. NO reduction by CO molecule over Si-doped boron nitride nanosheet: A dispersion-corrected DFT study. *Chem. Phys. Lett.* **2018**, *695*, 131–137. [CrossRef]
61. Roy, S.; Baiker, A. NO_x storage-reduction catalysis: From mechanism and materials properties to storage-reduction performance. *Chem. Rev.* **2009**, *109*, 4054–4091. [CrossRef]
62. Rosca, V.; Duca, M.; de Groot, M.T.; Koper, M.T. Nitrogen cycle electrocatalysis. *Chem. Rev.* **2009**, *109*, 2209–2244. [CrossRef]
63. Hu, Y.H.; Griffiths, K.; Norton, P.R. Surface science studies of selective catalytic reduction of NO: Progress in the last ten years. *Surf. Sci.* **2009**, *603*, 1740–1750. [CrossRef]
64. Zhang, X.; Lu, Z.; Tang, Y.; Fu, Z.; Ma, D.; Yang, Z. A density function theory study on the NO reduction on nitrogen doped graphene. *Phys. Chem. Chem. Phys.* **2014**, *16*, 20561–20569. [CrossRef] [PubMed]
65. Wang, Y.Y.; Zhang, D.J.; Yu, Z.Y.; Liu, C.B. Mechanism of N_2O Formation During NO Reduction on the Au(111) Surface. *J. Phys. Chem. C* **2010**, *114*, 2711–2716. [CrossRef]
66. Liu, Z.P.; Jenkins, S.J.; King, D.A. Why is silver catalytically active for NO reduction? A unique pathway via an inverted $(NO)_2$ dimer. *J. Am. Chem. Soc.* **2004**, *126*, 7336–7340. [CrossRef] [PubMed]
67. Liu, X.; Sheng, L. Al-Embedded C_2N: A DFT study on a promising catalyst for CO oxidation. *New J. Chem.* **2022**, *46*, 9250–9257. [CrossRef]
68. Tang, Y.; Yang, Z.; Dai, X. A theoretical simulation on the catalytic oxidation of CO on Pt/graphene. *Phys. Chem. Chem. Phys.* **2012**, *14*, 16566–16572. [CrossRef] [PubMed]